# Surface Charges of K Channels

## *Effects of Strontium on Five Cloned Channels Expressed in Xenopus Oocytes*

FREDRIK ELINDER,* MICHAEL MADEJA,‡ and PETER ÅRHEM*

From the *Nobel Institute for Neurophysiology and Department of Neuroscience, Karolinska Institutet, S-171 77 Stockholm, Sweden; and ‡Institut für Physiologie, D-48149 Münster, Germany

ABSTRACT The effects of strontium ($Sr^{2+}$; 7–50 mM) on five different cloned rat K channels (Kv1.1, Kv1.5, Kv1.6, Kv2.1, and Kv3.4), expressed in oocytes of *Xenopus laevis*, were investigated with a two-electrode voltage clamp technique. The main effect was a shift of the $G_K(V)$ curve along the potential axis, different in size for the different channels. Kv1.1 was shifted most and Kv3.4 least, 21 and 8 mV, respectively, at 50 mM. The effect was interpreted in terms of screening of fixed surface charges. The estimated charge densities ranged from −0.37 (Kv1.1) to −0.11 (Kv3.4) $e\,nm^{-2}$ and showed good correlation with the total net charge of the extracellularly located amino acid residues of the channel as well as with the charge of a specific region (the loop between the S5 segment and the pore forming segment). The estimated surface potentials were found to be linearly related to the activation midpoint potential, suggesting a functional role for the surface charges.

KEY WORDS: voltage clamp • voltage-gated channels • rat K channels

## INTRODUCTION

Metal ions are known to shift the open probability curves of most voltage-gated ion channels (Frankenhaeuser and Hodgkin, 1957; Hille et al., 1975; see also Hille, 1992). This effect has partly been attributed to screening of surface charges (see McLaughlin 1989; Hille 1992). In an earlier investigation of the channels in myelinated axons of *Xenopus laevis* (Elinder and Århem, 1994*a*, *b*), we have suggested that these surface charges mainly consist of the charged amino acids of the extracellular portion of the channel. Obviously, a critical test of this suggestion would be to analyze metal ion–induced shifts on channels, the molecular identity of which is known in detail. The present investigation is such a test. We have analyzed the effects of external strontium ($Sr^{2+}$) on five identified rat K channel types expressed in *Xenopus laevis* oocytes. The channels used are all voltage gated and belong to the Kv family: Kv1.1, Kv1.5, Kv1.6, Kv2.1, and Kv3.4 (for the nomenclature see Gutman and Chandy, 1993). Except for Kv3.4, which is relatively fast inactivating and has been characterized as an A channel, all channels have been characterized as delayed rectifiers (Frech et al., 1989; Stühmer et al., 1989; Grupe et al., 1990; Swanson et al., 1990; Rettig et al., 1992). The alkaline earth metal $Sr^{2+}$ was chosen for this investigation because it has been reported to shift voltage-dependent parameters along the potential axis relatively less than most other investigated metal ions (the exception is $Mg^{2+}$), and been suggested to mainly screen fixed surface charges with little or no binding (Hille et al., 1975; Århem, 1980; Cukierman and Krueger, 1990). The analysis revealed a clear correlation between the shift effects and the net charge of the extracellular loops of the channels, supporting the proposed hypothesis (Elinder and Århem, 1994*b*). Ways to extend the hypothesis by determining which extracellular loop is the main determinant for the effective charge density are discussed.

Address correspondence to Peter Århem, The Nobel Institute for Neurophysiology, Karolinska Institutet, S-171 77 Stockholm, Sweden. Fax: 46-8-34-95-44; E-mail: peter.arhem@neuro.ki.se

## MATERIALS AND METHODS

The experiments were performed at the Department of Physiology, Münster University. The present analysis is based on recordings from 34 cells (two donors), 18 of which were selected for the detailed quantitative analysis due to their stable recording conditions.

### *Synthesis of cRNA and Expression of Channels*

The cRNA for channels Kv1.1, Kv1.5, Kv1.6, Kv2.1, and Kv3.4 (Pongs, 1992) was synthesized by using the plasmid pAS18 as template for SP6 polymerase (Stühmer et al., 1988). The cRNA was stored at −20°C until injection. The oocytes of the South African clawed frog (*Xenopus laevis*) were used as the expression system. Frogs were anesthetized in ethyl *m*-aminobenzoate (Sandoz Pharmaceutical Ltd., Basel, Switzerland), and small sections of the ovary were removed surgically. Oocytes in stage V or VI (Dumont, 1972) were isolated manually from the ovary and injected with 1 ng of the respective cRNA in 50 nl distilled water. The injected oocytes were maintained under tissue culture conditions at 20°C until used for experiments. Experiments for the quantitative analysis were done from day 2 to 5 after injection of cRNA.

### *Electrophysiological Techniques*

The investigations were performed with the two-electrode voltage-clamp technique. Voltage pulses of 500-ms duration were ap-

plied from a holding potential of −80 mV to potentials from −70 to +60 mV in steps of 10 mV. The resulting currents were low pass filtered at 1 kHz. The volume bath resistance was between 0.5 and 1 kΩ. The resulting error of the shift values was estimated to be less than one millivolt. No series resistance compensation was therefore used. Microelectrodes were made from borosilicate glass and filled with a 3 M KCl solution. The resulting resistance varied between 0.5 and 2.0 MΩ. All experiments were carried out at room temperature (22 ± 1°C).

### *Solutions*

The tissue culture solution was a modified Barth medium (in mM): NaCl 88, KCl 1, $CaCl_2$ 1.5, $NaHCO_3$ 2.4, $MgSO_4$ 0.8; HEPES 5, pH 7.4, which was supplemented with penicillin (100 IU/ml) and streptomycin (100 μg/ml). In the electrophysiological experiments the control bath consisted of Ringer solution (in mM): NaCl 115, KCl 2, $CaCl_2$ 1.8, HEPES 10, pH 7.2. Strontium chloride ($Sr^{2+}$) was added to the bath solution in concentrations of 7, 20, and 50 mM. $Sr^{2+}$ was applied at least 20 s before eliciting the first voltage step. All solutions were applied with a concentration clamp technique (Madeja et al., 1991).

### *Theoretical Analysis*

The amplitudes of the total outward currents were corrected for leakage to obtain pure K currents. The leakage current was estimated from measurements at voltage steps of ±10 mV from the holding potential and the assumption of a linear leakage *I(V)* curve. The contribution of leakage currents to outward currents in the cRNA injected oocytes did not exceed 1% of the K current amplitude at a step to 0 mV.

The charge density (σ) was calculated by fitting the experimental data to the Grahame (1947) equation:

$$\sigma^2 = 2\varepsilon_r\varepsilon_0 RT\sum_{i=1}^{n} c_i\left[\exp\left(-z_i F\psi_0 R^{-1}T^{-1}\right)-1\right], \qquad (1)$$

where $\varepsilon_r$ is the dielectric constant of the membrane, $\varepsilon_0$ is the permittivity of free space, $c_i$ is the bulk concentration and $z_i$ is the valence of the *i*th ionic species in the extracellular solution, *n* is the number of ionic species, and $\psi_0$ is the external membrane surface potential. *R*, *T*, and *F* have their usual thermodynamic significance. Although Eq. 1 is strictly valid only for a uniformly smeared charge, it has been shown that the equation can be used as an approximation for charge densities more negative than $-0.16\ e\ nm^{-2}$ (Peitzsch et al., 1995). In the present investigation the charge densities analyzed were found mainly to be more negative than this value, thus allowing the use of Eq. 1.

The K conductance $G_K(V)$ was calculated as:

$$G_K(V) = I_K(V)/(V-E_K), \qquad (2)$$

where $I_K(V)$ is the K current, $V$ is the absolute membrane potential, and $E_K$ is the equilibrium potential, assumed to be −80 mV (Dascal, 1987). The inward tail currents at −80 mV seen in the experiments (see Fig. 1) suggest that $E_K$ is slightly less negative. However, this deviation will only marginally affect the estimation of the $Sr^{2+}$-induced shifts of the $G_K(V)$ curves in the present investigation. Assuming $E_K$ to be −100 or −60 mV will change the estimated shifts (based on the assumption of $E_K = -80$ mV) by <1 mV.

## RESULTS

Fig. 1 shows current families in control (Ringer) solution and in 50 mM $Sr^{2+}$ solution, respectively, for the five channel types used in the present investigation. The delayed rectifier character of the Kv1.1, 1.5, 1.6, and 2.1 channels and the fast inactivation of the Kv3.4 channel are evident. It can also be seen that the potential range of activation differs between the channel types: Kv1.1 activates at most negative and Kv3.4 at most positive potentials. This channel-dependent activation potential difference is more easily seen in Fig. 2 where the current vs. potential *I(V)* and conductance vs. potential *G(V)* curves are shown.

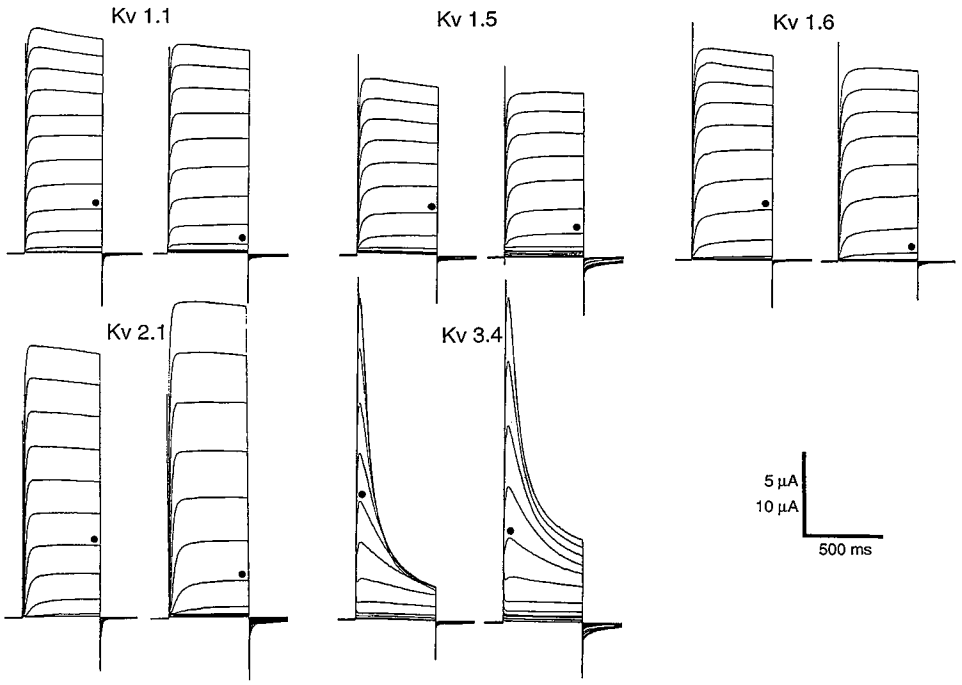


FIGURE 1. Effects of 50 mM $Sr^{2+}$ on current families for the K channels studied. Control conditions on the left and test conditions on the right. Voltage steps up to +60 mV in steps of 10 mV from a holding potential of −80 mV. Vertical scale bar for Kv2.1 is 10 μA, for the others 5 μA. To make the shift effect clear, currents at the same potential in control and test solution are marked with dots (−20, 0, −10, 0, and +20 mV, respectively).

As also seen from Fig. 1, $Sr^{2+}$ shifts the potential at which the channel is activated in positive direction while the currents at the highest potentials remain relatively intact. This shift of activation potential differs for the different channel types; the largest being that of Kv1.1 and the smallest that of Kv3.4. The shifts are more evident in Fig. 2, where the $Sr^{2+}$ effect on *I(V)* and *G(V)* curves is depicted.

Fig. 1 also shows that $Sr^{2+}$ affects the tail currents at repolarization of all five channels and the inactivation of Kv3.4. The inactivation modification consists of a slower time course and an increased steady-state value (at 50 mM $Sr^{2+}$ the time constant as well as the steady-state value were approximately doubled). The tail current effect consists of an increased amplitude, the magnitude of which differing between the different channel types. While the modified inactivation may partly be explained by a modified voltage dependence as reflected by the shift effect, the tail current modification seems not to be so; the effect being largest for Kv1.5 and Kv3.4, which show the smallest shifts. Thus, the effect on the current tails seems caused by another mechanism than that causing the shift effect and will not be further analyzed here.

All the $Sr^{2+}$ effects described in the present investigation, except for the $Sr^{2+}$-induced reduction of current at the most positive potentials in Kv1.1 experiments, were perfectly reversible. The current reduction for Kv1.1 was, unexpectedly, increased after application of control solution while the shift was reversible. The difference in reversibility between the reduction and the shift suggests that they are unrelated.

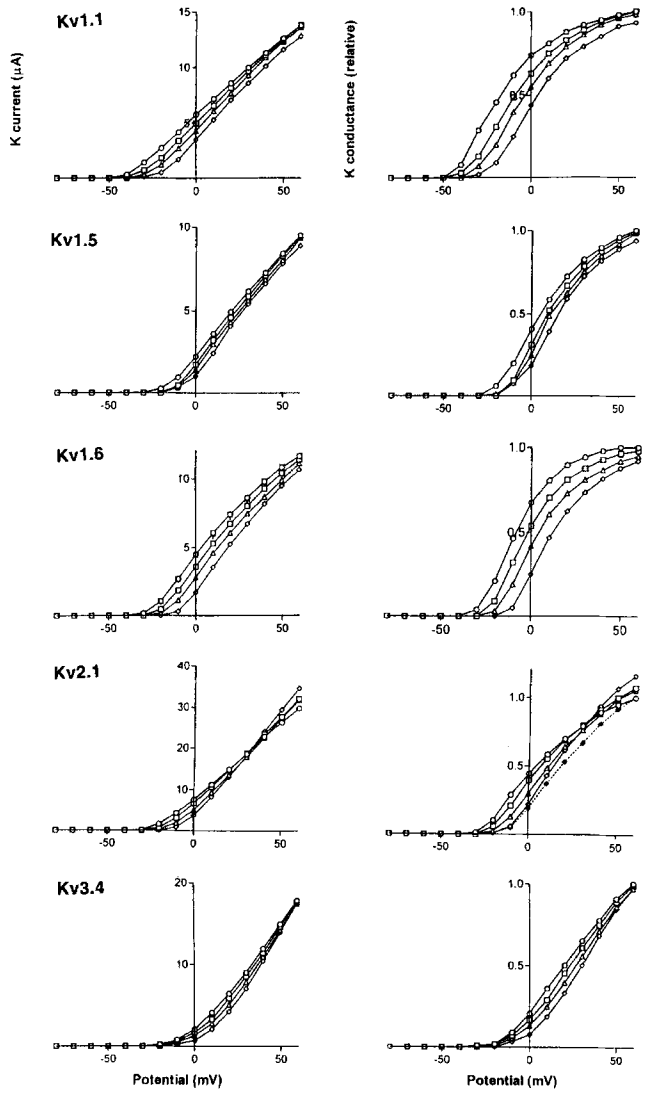


FIGURE 2. Effects of $Sr^{2+}$ on *I(V)* and corresponding *G(V)* curves for the K channels studied. Current measured as maximum current. Same cells as in Fig. 1. Control (○), 7 mM $Sr^{2+}$ (□), 20 mM $Sr^{2+}$ (△), and 50 mM $Sr^{2+}$ (◇). For Kv2.1 the values for 50 mM $Sr^{2+}$ are scaled (◆) to fit control at +60 mV.

### *Shift of Conductance Curves*

Fig. 2 shows the *I(V)* curves (*left*) and corresponding *G(V)* curves at three concentrations $Sr^{2+}$ (7, 20, and 50 mM) for the five channel types investigated. The current values shown are maximum values, that is near steady-state values in the case of the non-inactivating channels Kv1.1, Kv1.5, Kv1.6, and Kv2.1 and peak values in the case of the inactivating Kv3.4 channel.

The *G(V)* curves clearly show the different activation potentials for the different channels, the most negative being that for Kv1.1 and the most positive for Kv3.4. The midpoint values from 18 cells are collected in Table I. The *G(V)* curves in Fig. 2 also reveal that for four of the channels depicted, the effect of $Sr^{2+}$ is almost a pure (dose-dependent) shift. For Kv2.1 the effect is a shift in combination with an almost potential-independent increase (described by a scaling factor). This increase was systematic and reversible; in three experiments at 50 mM $Sr^{2+}$, *G* at +60 mV increased 20 ± 12%

TABLE I

*Midpoint Values and Strontium-induced Shifts: Experimentally and Theoretically Estimated Charge Densities*

| Channel Type | $V_{1/2}$ | Shifts | | | Charge density | |
|---|---|---|---|---|---|---|
| | | 7 mM | 20 mM | 50 mM | exp. | theor. |
| | *mV* | | *mV* | | *e nm*$^{-2}$ | |
| Kv1.1 (*n* = 5) | −17 ± 1 | 7.6 ± 0.5 | 13.6 ± 0.2 | 20.8 ± 0.5 | −0.37 | −0.50 |
| Kv1.5 (*n* = 3) | +1 ± 3 | 3.7 ± 0.3 | 6.7 ± 0.3 | 12.0 ± 1.0 | −0.17 | −0.16 |
| Kv1.6 (*n* = 3) | −5 ± 2 | 5.7 ± 0.9 | 11.0 ± 0.6 | 17.3 ± 1.2 | −0.28 | −0.56 |
| Kv2.1 (*n* = 4) | +5 ± 1 | 3.5 ± 0.3 | 7.0 ± 0.0 | 12.0 ± 0.4 | −0.17 | −0.06 |
| Kv3.4 (*n* = 3) | +17 ± 2 | 2.7 ± 0.3 | 5.0 ± 0.6 | 7.7 ± 0.7 | −0.11 | +0.09 |

All values are mean ± SEM. The experimental charge densities are calculated from the shifts with Eq. 1. Theoretical charge densities are calculated as net charge of extracellular loops divided by a subunit area of 16 nm$^2$ (Li et al., 1994).

(mean ± SD). The cause of this increase is unclear. For another channel, Kv1.1, the shift of the *G(V)* curve was in some experiments (exclusively in cells tested within 3 d after RNA injection) combined with a marked reduction at the highest potentials. The reduction of 50 mM $Sr^{2+}$ at +60 mV in six experiments was 20 ± 14% (mean ± SD). As mentioned above, this reduction was even more pronounced in the control solution applied after the application of the $Sr^{2+}$ solution. The reduction in control solution after application of 50 mM $Sr^{2+}$ was 37 ± 13% (mean ± SD; $n = 7$). This phenomenon clearly needs further detailed investigation. However, as argued above (the difference in reversibility), it seems unrelated to the shift effect and will not be treated further in this paper.

The effects on Kv1.5, 1.6, and 3.4 were completely reversible; the *I(V)* curves in control solution before and after application of test solution completely overlapped (not shown). The effect on Kv1.1 was also perfectly reversible with respect to the most negative potentials of the *I(V)* curve. For Kv2.1, however, the control curves during an experiment showed some drift: the midpoint potential of the *G(V)* curve could vary up to 5 mV in either direction.

To quantify the shifts of the *G(V)* curves, values were estimated at 25% of the maximum level. By this procedure, interference by scaling effects as well as by potential-dependent effects (mainly in the Kv1.1 experiments) was minimized. In the Kv2.1 experiments, which showed the largest scaling effects, interference was avoided by normalizing the *G(V)* curves, assigning *G* at +60 mV the value 1.0. To account for the drift of the *G(V)* curves in the Kv2.1 experiments, the shift values were measured relative to the mean of the control value before and after application of test solution. The collected values from 18 experiments are listed in Table I.

### *Shifts of Time Constant Curves*

The shift data in Table I were used to calculate the effective charge densities for the different channels. Assuming that the mechanism underlying the shift effect is exclusively screening (involving no binding), the charge density is obtained directly by fitting shift data to the Grahame equation (Eq. 1). $Sr^{2+}$ has been suggested to affect voltage-gated channels by mainly screening in a number of preparations (see INTRODUCTION). This was the reason for the choice of $Sr^{2+}$ for the present study. To test wether the assumption of screening also applies to the studied preparation the effect on the curve describing time to half maximum current ($t_{1/2}$) vs. potential curve was compared with the effect on the *G(V)* curve. A pure screening effect predicts that the $t_{1/2}(V)$ and the *G(V)* curves are shifted equally. A binding effect, on the other hand, is, in addition, likely to directly affect the gating due to the short distances involved and, consequently, is expected to affect the *G(V)* and $t_{1/2}(V)$ curves differently (for a discussion see Elinder and Århem, 1994*b*). Fig 3. shows the $t_{1/2}(V)$ curves for the studied channels in control solution (*open circles*) and in 50 mM $Sr^{2+}$ (*squares*) for the same experiments as in Figs. 1 and 2. To simplify a comparison between the magnitude of the $t_{1/2}(V)$ curve shifts and of the *G(V)* curve shifts, the figure shows the control $t_{1/2}(V)$ curves shifted with the values obtained from the *G(V)* curves in Fig. 2 (*filled circles*). The agreement is striking for all channel types, thus supporting the assumption of a screening induced shift effect.

### *Estimation of Surface Charge Densities*

The shift values (collected in Table I) could thus be used to directly estimate the effective charge density by the Grahame equation (Eq. 1) and a least square proce-

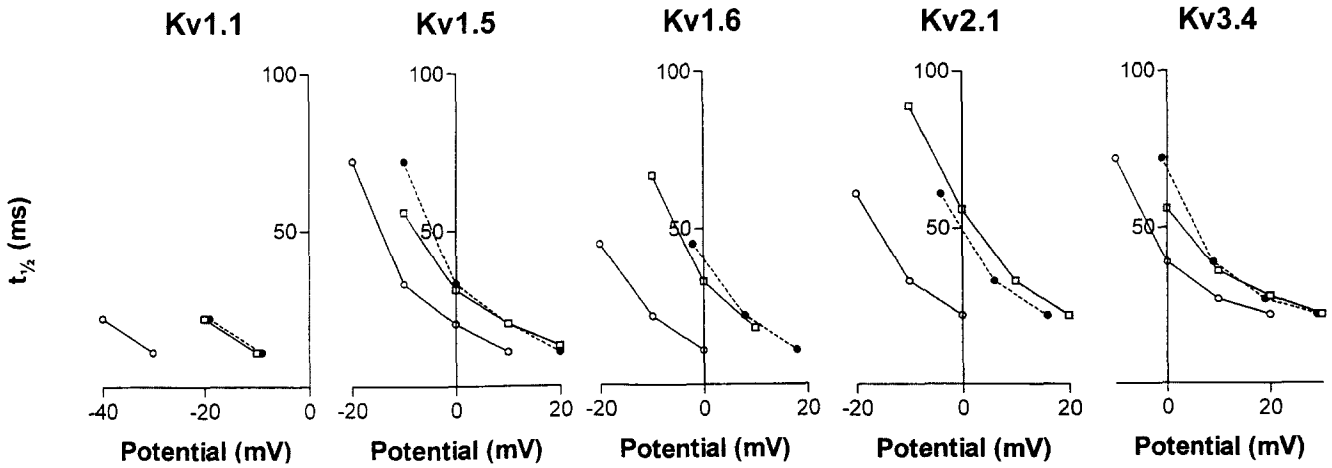


FIGURE 3. Effect of 50 mM $Sr^{2+}$ on $t_{1/2}(V)$ curves for the K channels studied. Control (○) and $Sr^{2+}$ (□) solutions. Control curve shifted the same amount as the *G(V)* curve in Fig. 2 (●).

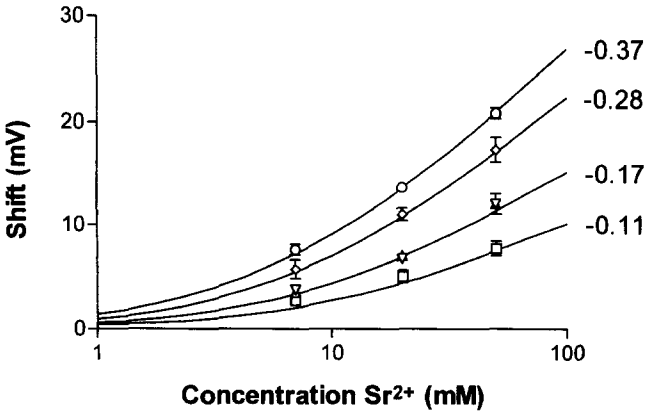


FIGURE 4. Shifts of $G(V)$ curves versus $Sr^{2+}$ concentration for the K channels studied. (○) Kv1.1, (▽) Kv1.5, (◇) Kv1.6, (△) Kv2.1, and (□) Kv3.4. Data from Table 1. The fitted curves are least square fitted solutions to Eq. 1 for different values of surface charge density as indicated ($e\,nm^{-2}$).

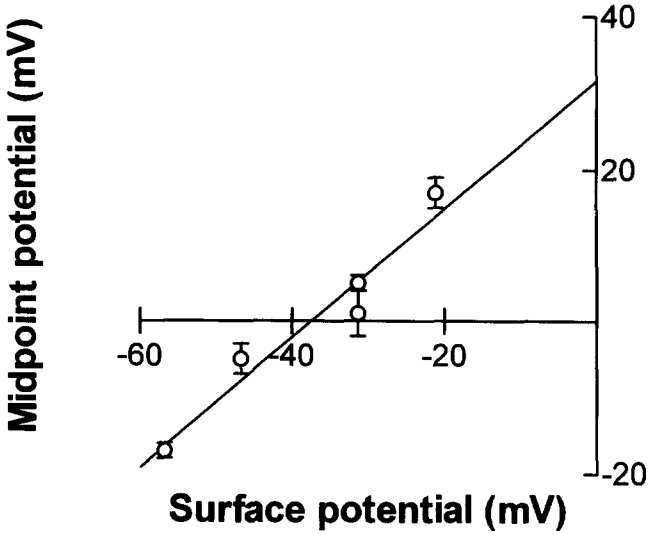


FIGURE 5. Midpoint potential ($V_{1/2}$) versus surface potential ($\psi_0$) for the K channels studied. Data from Table I. $\psi_0$ is calculated from Eq. 1. Straight line is least-square fitted to the data points ($r^2$ = 0.94). The slope is 0.86 and y-axis crossing point +32 mV.

dure. Fig. 4 shows the best fits, yielding charge densities of −0.37, −0.28, −0.17, −0.17, and −0.11 $e\,nm^{-2}$ for Kv1.1 (*circles*), Kv1.6 (*diamonds*), Kv1.5 (*inverted triangles*), Kv2.1 (*triangles*), and Kv3.4 (*squares*), respectively. The estimated charge densities are listed in Table I.

From the fact that the estimated charge densities differ for the different channels, it is immediately clear that the channel protein as such is essential for the effect (c.f. Cukierman et al., 1988). A comparison with values estimated from primary structures will be performed below.

Table I also shows estimated midpoint values for the different channel types. These values correlate reasonably well with the estimated charge densities, the value for Kv1.1 being most negative (−17 mV) and that of Kv3.4 most positive (+17 mV). Fig. 5 shows the relation expressed as midpoint values vs. surface potential obtained from the Grahame equation (Eq. 1). The relation is linear with a (least square fitted) midpoint value of +32 mV at a surface potential of 0 mV and a slope of 0.86 ($r^2$ = 0.94), suggesting a direct relation between the surface charge density and the gating process. The interpretation of this fact will be dealt with in the DISCUSSION.

*Relation to Molecular Biology Data*

The central aim of the present study was to analyze the hypothesis proposed in an earlier investigation (Elinder and Århem, 1994*b*) that the charged extracellular loops of the channel protein determine the effective charge density. In Table I the experimentally estimated charge densities are listed together with the charge densities calculated from the primary structures. The primary structure value was calculated as the sum of the net charges of the four extracellular loops, i.e., the loops connecting the S1 and S2 segments (S1-S2), S3 and S4 (S3-S4), S5 and the pore forming (P) region (S5-P), and P and S6 (P-S6), divided by 16 $nm^2$, which is the subunit area recently found in studies of *Shaker* channels (Li et al., 1994). The sequences of the extracellular loops used and the charges assigned to the different amino acids are presented in Elinder and Århem (1994*b*) and in Elinder (1994).

A comparison between the experimental and the primary structure values shows that there is a positive correlation between the two sets (Table I). This correlation is illustrated more clearly in the left panel of Fig. 6 (*Total*). The least square-fitted straight line through the origin has a slope of 20.7 $nm^2$ ($r^2$ = 0.79).

Fig. 6 also shows the relation between the net charges and the estimated charge densities of the four individual loops of each channel type (Table II). For the S1-S2 loop, the least square-fitted straight line through the origin has a slope of 15.6 $nm^2$ ($r^2$ = 0.78), and for S5-P, the slope is 10.1 $nm^2$ ($r^2$ = 0.86). The two remaining loops S3-S4 and P-S6 show negative correlations, suggesting that they are not directly involved in the screening effect. In conclusion, the shown presentation of the data suggests that the experimentally estimated charge densities correlate positively with the total net charge, as well as with the net charge of both the S1-S2 loop and the S5-P loop. The question of which of these charged structures is the major determinant of the effective charge density is not possible to determine from the presented figure. Some ways to analyze this problem further will be discussed below.

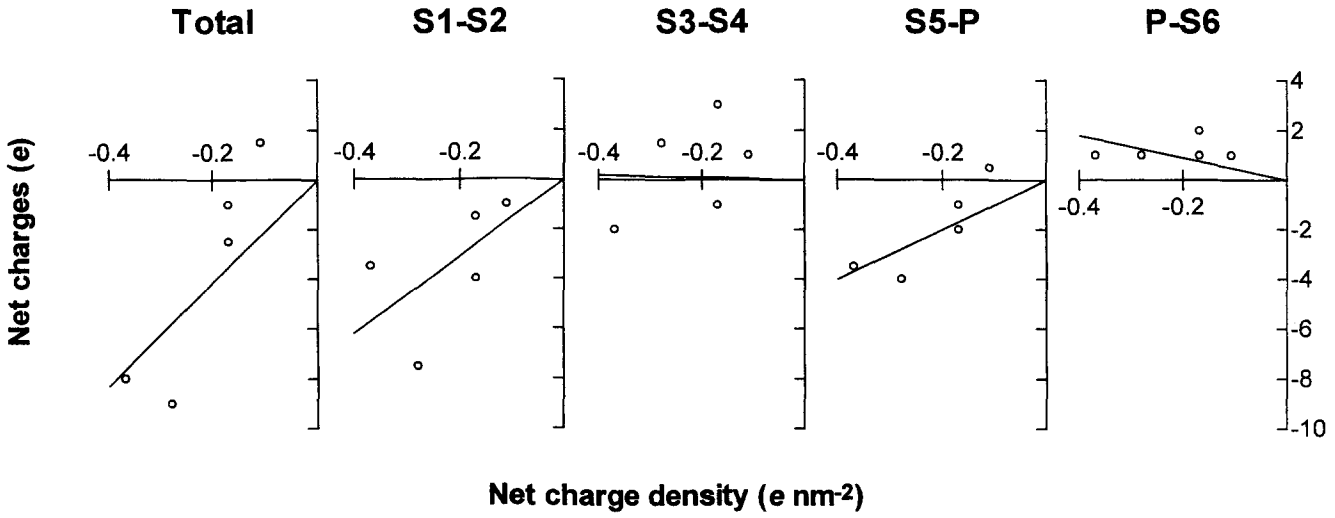


FIGURE 6. Net charge for the extracellular loops (as indicated) versus estimated charge density of the studied K channels. Definitions of the extracellular loops are given in Elinder and Århem (1994*b*) and in Elinder (1994). Slopes of the least square fitted lines are (from left to right): 20.7 $nm^2$ ($r^2 = 0.79$), 15.6 $nm^2$ ($r^2 = 0.78$), −0.5 $nm^2$, 10.1 $nm^2$ ($r^2 = 0.86$), and −4.5 $nm^2$. These values can be interpreted as the area that the loop would cover if the charges are uniformly smeared, and if the loop is the exclusive determinant of the estimated charge density.

## DISCUSSION

In the present investigation we have analyzed $Sr^{2+}$ effects on five identified cloned K channels. The main aim was to investigate the hypothesis that the extracellular portion of the channel protein determines the effective charge density (Elinder and Århem, 1994*b*). Thus the focus was on the induced shifts of *G(V)* curves. In conclusion, the investigation supports the proposed hypothesis. However, the question of whether all extracellular loops or whether some specific loop is the critical determinant needs further clarification and will be discussed below. In addition, we will discuss a possible role of the charges for the gating of channels, based on the observed correlation between midpoint value of the activation curve and calculated surface potential for the different channels.

### *The Determinants of the Effective Surface Charges*

From Fig. 6 it is clear that the experimentally estimated surface charge density correlates well with the total net charge as well as with the net charge of the S1-S2 loop and the S5-P loop. A comparative analysis of different Kv1 channels suggests that the S1-S2 loop does not influence the channel properties (Grupe et al., 1990; see also Elinder and Århem, 1994*b*). The question is then whether the S5-P loop is a better determinant of the charge density than the total extracellular net charge. This was not possible to determine from the results in the present study. However, a way to get information on this issue is outlined below. Fig. 7 shows the relation between total net surface charge and the net charge of the S5-P loop for a number of cloned K channels (the presently analyzed channels indicated by filled squares; references taken from Gutman and Chandy, 1993; sequences listed in Elinder, 1994). As seen, the relation can be approximated as linear. The least square-fitted line through the origin ($r^2 = 0.73$) has a slope of 0.43, implying that about half of the total net charge is located on the relatively short S5-P loop. However, as indicated in the figure there are some striking exceptions (*encircled symbols*). One is the xKv1.1 channel of *Xenopus laevis*, and another is the *ShakerB* channel from *Drosophila melanogaster*. The S5-P loop of xKv1.1 (−5.5/−4.5) is more charged than expected from the regression line and *ShakerB* (−7.5/−1.0) less. This means that these channels can be used to discriminate between the alternatives of the total net charge or the net charge of the S5-P loop as main determinant of the effective surface charge density. The two alternatives predict highly different ($Mg^{2+}$ and $Sr^{2+}$ induced) shift values for these channels.

The discussion above is based on the assumption that mainly charged amino acid residues determine the

TABLE II

*Net Charge of the Extracellular Loops*

| Channel Type | S1-S2 | S3-S4 | S5-P | P-S6 | Total |
|---|---|---|---|---|---|
| Kv1.1 | −3.5 | −2 | −3.5 | +1 | −8 |
| Kv1.5 | −1.5 | −1 | −1 | +1 | −2.5 |
| Kv1.6 | −7.5 | +1.5 | −4 | +1 | −9 |
| Kv2.1 | −4 | +3 | −2 | +2 | −1 |
| Kv3.4 | −1 | +1 | +0.5 | +1 | +1.5 |

Data from references cited in Gutman and Chandy (1993; see also Elinder and Århem, 1994*b*, and Elinder, 1994).

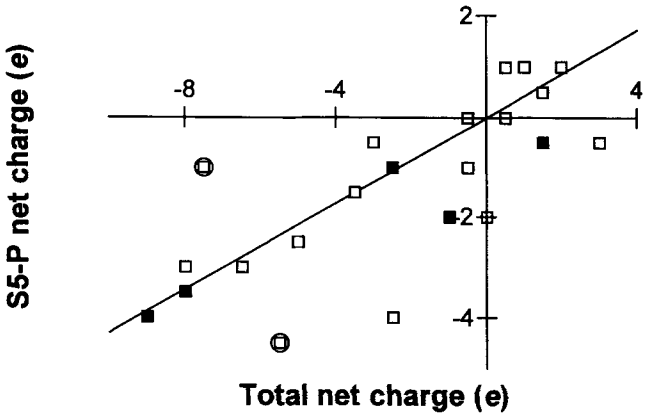


FIGURE 7. Net charge of all extracellular loops versus net charge of the S5-P loop for 23 different K channels (listed in Gutman and Chandy, 1993). The definitions of the extracellular loops are given in Elinder and Århem (1994*b*) and in Elinder (1994). Filled squares indicate the channels studied in the present investigation. The straight line through the origin is least-square fitted to all data points and has a slope of 0.43 ($r^2 = 0.73$). Symbols for deviating channels (discussed in the text) are surrounded by circles. Identification of data points: Kv1.1 (−8, −3.5), Kv1.2 (−6.5, −3), Kv1.3 (−8, −3), Kv1.4 (−5, −2.5), Kv1.5 (−2.5, −1), Kv1.6 (−9, −4), Kv2.1 (−1, −2), Kv2.2 (0, −2), Kv3.1 (−0.5, 0), Kv3.2 (−3, −0.5), Kv3.3 (−3.5, −1.5), Kv3.4 (+1.5, +0.5), Kv4.1 (+1, +1), Kv4.2 (+0.5, +1), Kv4.3 (+2, +1), Kv5.1 (−0.5, −1), Kv6.1 (−2.5, −4), xKv1.1 (−5.5, −4.5), xKv1.2 (−6.5, −3), Shaker (−7.5, −1), Shab (−0.5, −1), Shaw (+3, −0.5), Shal (+0.5, 0).

functional charge density. In some investigations sialic residues attached to asparagine(N)-linked oligosaccharide chains have been suggested to play a major role as surface charges (Recio-Pinto et al., 1990). However, this seems not be the case in the studied channels, because (*a*) there seems to be no correlation between estimated charge density and number of putative sites (Table III) and (*b*) removal of these carbohydrate moieties by site-directed mutagenesis show that they exert negligible effects on surface charges and gating (Santacruz-Toloza et al., 1994; Bennet et al., 1994; Talukder et al., 1994).

*Midpoint Activation Curve Values and Surface Charges*

It is well known that the activation midpoint potential seems unrelated to the charge of the putative gating segment of the channel; electroneutral point mutations of the S4 segment can markedly affect the midpoint value (Papazian et al., 1991). Nevertheless we find the linear relation between midpoint values and surface potentials (Fig. 5) intriguing. This relation may

TABLE III

*Putative Glycosylation Sites in the Extracellular Loops and Experimentally Obtained Charge Densities*

| Channel Type | S1-S2 | S3-S4 | S5-P | P-S6 | Total | Charge Density |
|---|---|---|---|---|---|---|
| | | | | | | $e\ nm^{-2}$ |
| Kv1.1 | 1 | 0 | 0 | 0 | 1 | −0.37 |
| Kv1.5 | 1 | 0 | 0 | 0 | 1 | −0.17 |
| Kv1.6 | 0 | 0 | 0 | 0 | 0 | −0.28 |
| Kv2.1 | 0 | 1 | 0 | 0 | 1 | −0.17 |
| Kv3.4 | 2 | 0 | 0 | 0 | 2 | −0.11 |

Data from references cited in Gutman and Chandy (1993; see also Elinder, 1994).

suggest a functional role for extracellular fixed charges in the gating process in native channels. It further suggests information about the influence of electrical and non-electrical forces on the voltage sensor of native channels. As shown in Fig. 5 the estimated midpoint value at 0 mV surface potential is +32 mV. An overview of gating current properties described in the literature reveals that the midpoint value of the gating charge curve is about 20 mV more negative than that of the channel activation curve (Hille, 1992; Keynes, 1994). A midpoint value of +32 mV would then mean a midpoint potential of the gating charge curve of +12 mV. Assuming an intracellular surface potential of about −20 to −10 mV relative intracellular bulk potential (see Chandler et al., 1965; Hille, 1992), this means that the midpoint of the gating charge curve for the studied channels would be about 0 mV in the absence of internal and external surface charges. This would suggest that non-electrical forces on the voltage sensor are symmetrical.

*Concluding Remarks*

In conclusion, the present study supports the hypothesis (Elinder and Århem, 1994*b*) that the charge profile of the extracellular surface of the channel protein plays an important role for determining the effective surface charge density of the channel. Obviously, a further step in the analysis would be to perform mutation studies. However, simple point mutations may not easily yield conclusive results due to the linear relationship between the net charge of the interesting loops (mainly S5-P) and the total net charge of the studied channels. Studies of native channels with deviating charge profiles (Fig. 7) were therefore suggested as a more immediate way to get information about the issue.

We are grateful to Professor O. Pongs (University of Hamburg, Hamburg, Germany) for providing cRNA probes coding for the K channels and to Dr. R. Hill for valuable comments on the manuscript.

This work was supported by grants from the Swedish Medical Research Council (project 6552) and Karolinska Institutets Fonder.

*Original version received 22 April 1996 and accepted version received 1 July 1996.*

REFERENCES

Århem, P. 1980. Effects of some heavy metal ions on the ionic currents of myelinated fibers from *Xenopus laevis*. *J. Physiol. (Lond.)*. 306:219–231.

Bennet, E., V.V. Patel, S.S. Tinkle, M.S. Urcan, and S.R. Levinson. 1994. Effects of N-glycosylation on sodium channel gating. *Biophys. J.* 66:A102 (Abstr.).

Chandler, W.K., A.L. Hodgkin, and H. Meves. 1965. The effect of changing the internal solution on sodium inactivation and related phenomena in giant axons. *J. Physiol. (Lond.)*. 180:821–836.

Cukierman, S., and B.K. Krueger. 1990. Modulation of sodium channel gating by external divalent cations: differential effects on opening and closing rates. *Pflügers Arch.* 416:360–367.

Cukierman, S., W.C. Zinkand, R.J. French, and B.K. Krueger. 1988. Effects of membrane surface charge and calcium on the gating of rat brain sodium channels in planar bilayers. *J. Gen. Physiol.* 92: 431–447.

Dascal, N. 1987. The use of *Xenopus* oocytes for the study of ion channels. *CRC Crit. Rev. Biochem.* 22:317–387.

Dumont, J.M. 1972. Oogenesis in *Xenopus laevis* (Daudin). I. Stages of oocyte development in laboratory maintained animals. *J. Morphol.* 136:153–179.

Elinder, F. 1994. Surface charges of voltage-gated ion channels. Doctoral thesis, Karolinska Institutet, Stockholm. 39 pp.

Elinder, F., and P. Århem. 1994*a*. Effects of gadolinium on ion channels in the myelinated axon of *Xenopus laevis*: four sites of action. *Biophys. J.* 67:71–83.

Elinder, F., and P. Århem. 1994*b*. The modulatory site for action of gadolinium on surface charges and channel gating. *Biophys. J.* 67: 84–90.

Frankenhaeuser, B., and A.L. Hodgkin. 1957. The action of calcium on the electrical properties of squid axons. *J. Physiol. (Lond.)*. 137:218–244.

Frech, G.C., A.M.J. VanDongen, G. Schuster, A.M. Brown, and R.H. Joho. 1989. A novel potassium channel with delayed rectifier properties isolated from rat brain by expression cloning. *Nature (Lond.)*. 340:642–645.

Grahame, D.C. 1947. The electrical double layer and the theory of electrocapillarity. *Chem. Rev.* 41:441–501.

Grupe, A., K.H. Schröter, J.P. Ruppersberg, M. Stocker, T. Drewes, S. Beckh, and O. Pongs. 1990. Cloning and expression of a human voltage-gated potassium channel. A novel member of the RCK potassium channel family. *EMBO (Eur. Mol. Biol. Organ.) J.* 9: 1749–1756.

Gutman, G.A., and K.G. Chandy. 1993. Nomenclature of mammalian voltage-dependent potassium channel genes. *Sem. Neurosci.* 5:101–106.

Hille, B. 1992. Ionic Channels of Excitable Membranes. 2nd ed. Sinauer Associates Inc., Sunderland, MA. 612 pp.

Hille, B., A.M. Woodhull, and B.I. Shapiro. 1975. Negative surface charge near sodium channels of nerve: divalent ions, monovalent ions, and pH. *Phil. Trans. R. Soc. Lond. B.* 270:301–318.

Keynes, R.D. 1994. The kinetics of voltage-gated ion channels. *Q. Rev. Biophys.* 27:339–434.

Li, M., N. Unwin, K.A. Stauffer, Y.N. Jan and L.Y. Jan. 1994. Images of purified *Shaker* potassium channels. *Curr. Biol.* 4:110–115.

Madeja, M., U. Musshoff, and E.-J. Speckmann. 1991. A concentration-clamp system allowing two-electrode voltage-clamp investigations in oocytes of *Xenopus laevis*. *J. Neurosci. Methods.* 38:267–269.

McLaughlin, S. 1989. The electrostatic properties of membranes. *Annu. Rev. Biophys. Chem.* 18:113–136.

Papazian, D.M., L.C. Timpe, Y.N. Jan, and L.Y. Jan. 1991. Alteration of voltage dependence of *Shaker* potassium channel by mutations in the S4 sequence. *Nature (Lond.)*. 349:305–310.

Peitzsch, R.M., M. Eisenberg, K.A. Sharp, and S. McLaughlin. 1995. Calculation of the electrostatic potential adjacent to model phospholipid bilayers. *Biophys. J.* 68:729–738.

Pongs, O. 1992. Molecular biology of voltage-dependent potassium channels. *Physiol. Rev.* 72:S69–S88.

Recio-Pinto, E., W.B. Thornhill, S. Duch, S.R. Levinson, and B.W. Urban. 1990. Neuraminidase treatment modifies the function of electroplax sodium channels in planar lipid bilayers. *Neuron.* 5: 675–684.

Rettig, J., F. Wunder, M. Stocker, R. Lichtinghagen, F. Mastiaus, S. Beckh, W. Kues, P. Pedarzani, K.H. Schröter, J.P. Ruppersberg, et al. 1992. Characterization of a Shaw-related potassium channel family in rat brain. *EMBO (Eur. Mol. Biol. Organ.) J.* 11:2473–2486.

Santacruz-Toloza L., Y. Huang, S.A. John, and D.M. Papazian. 1994. Glycosylation of *Shaker* potassium channel protein in intact cell culture and in *Xenopus* oocytes. *Biochemistry.* 33:5607–5613.

Stühmer, W., J.P. Ruppersberg, K.H. Schröter, B. Sakmann, M. Stocker, K.P. Giese, A. Perschke, A. Baumann, and O. Pongs. 1989. Molecular basis of functional diversity of voltage-gated potassium channels in mammalian brain. *EMBO (Eur. Mol. Biol. Organ.) J.* 8:3235–3244.

Stühmer, W., M. Stocker, B. Sakmann, P. Seeburg, A. Baumann, A. Grupe, and O. Pongs. 1988. Potassium channels expressed from rat brain cDNA have delayed rectifier properties. *FEBS Lett.* 242: 199–206.

Swanson R., J. Marshall, J.S. Smith, J.B. Williams, M.B. Boyle, K. Folander, C.J. Luneau, J. Antanavage, J.C. Oliva, S.A. Buhrow, et al. 1990. Cloning and expression of cDNA and genomic clones encoding three delayed rectifier potassium channels in rat brain. *Neuron.* 4:929–939.

Talukder, G., S.J. Gibbons, M.M. Tamkun, and N.L. Harrison. 1994. Probing the site of $Zn^{2+}$ action using cloned and mutant voltage-gated $K^+$ channels. *Biophys J.* 66:A209 (Abstr.).